

## RET inhibition in novel patient-derived models of RET-fusion positive lung adenocarcinoma reveals a role for MYC upregulation

Takuo Hayashi<sup>1,2,3,\*</sup>, Igor Odintsov<sup>1,2,\*</sup>, Roger S. Smith<sup>1,2,4\*</sup>, Kota Ishizawa<sup>2,7</sup>, Allan J.W. Liu<sup>5,6</sup>, Lukas Delasos<sup>5</sup>, Christopher Kurzatkowski<sup>1</sup>, Huichun Tai<sup>1,2</sup>, Eric Gladstone<sup>1,2</sup>, Morana Vojnic<sup>1,2</sup>, Shinji Kohsaka<sup>1,2,8</sup>, Ken Suzawa<sup>1,9</sup>, Zebing Liu<sup>1,2,10</sup>, Siddharth Kunte<sup>5</sup>, Marissa S. Mattar<sup>11</sup>, Inna Khodos<sup>11</sup>, Monika A. Davare<sup>12</sup>, Alexander Drilon<sup>5</sup>, Emily Cheng<sup>2</sup>, Elisa de Stanchina<sup>11</sup>, Marc Ladanyi<sup>1,2,a,#</sup> and Romel Somwar<sup>1,2,a,#</sup>

<sup>1</sup>Department of Pathology, Memorial Sloan Kettering Cancer Center, New York, NY.

<sup>2</sup>Human Oncology and Pathogenesis Program, Memorial Sloan Kettering Cancer Center, New York, NY

<sup>3</sup>Current address: Department of Human Pathology, Graduate School of Medicine, Juntendo University, Bunkyo-ku, Tokyo, Japan

<sup>4</sup>Current address: Medical Scientist Training Program, Northwestern University Feinberg School of Medicine, Chicago, IL, USA.

<sup>5</sup>Thoracic Oncology Service, Division of Solid Tumor Oncology, Department of Medicine, Memorial Sloan Kettering Cancer Center, New York, NY.

<sup>6</sup>Faculty of Medicine, The Chinese University of Hong Kong, Shatin, NT, Hong Kong SAR, China

Antitumor Core Facility, Molecular Pharmacology Program, Memorial Sloan Kettering Cancer Center, New York, NY

<sup>7</sup>Current address: Department of Education and Support for Community Medicine, Tohoku Medical Megabank Organization, Tohoku University, Sendai, Japan

<sup>8</sup>Current address: Division of Cellular Signaling, National Cancer Center Research Institute, Tokyo, Japan

<sup>9</sup>Current address: Department of Thoracic, Breast and Endocrinological Surgery, Okayama University Graduate School of Medicine, Dentistry and Pharmaceutical Sciences, Okayama, Japan

<sup>10</sup>Current address: Department of Molecular Pathology, Renji Hospital, Medical School of Shanghai Jiao Tong University, Shanghai, China

<sup>11</sup>Anti-tumor Core Facility, Molecular Pharmacology Program, Memorial Sloan Kettering Cancer Center, New York, NY.

<sup>12</sup>Department of Pediatrics, Oregon Health Sciences University

\*These authors contributed equally to this study

<sup>a</sup>Co-senior authors

#Address correspondence to

Romel Somwar: [somwarr@mskcc.org](mailto:somwarr@mskcc.org)

Marc Ladanyi: [ladanyim@mskcc.org](mailto:ladanyim@mskcc.org)

Key words: *RET* fusion PDX, MYC, RET inhibitor, transcriptome, NSCLC

## Summary statement

We established four patient-derived models of RET fusion-positive lung adenocarcinomas with three different RET fusions. Using these models we show that MYC expression is regulated by RET.

## Abstract

Multi-kinase RET inhibitors, such as cabozantinib and RXDX-105, are active in lung cancer patients with *RET* fusions; however, the overall response rates to these two drugs are unsatisfactory compared to other targeted therapy paradigms. Moreover, these inhibitors may have different efficacies against *RET* rearrangements depending on the upstream fusion partner. A comprehensive preclinical analysis of the efficacy of RET inhibitors is lacking due to a paucity of disease models harboring *RET* rearrangements. Here we generated two new patient-derived xenograft (PDX) models, one new patient-derived cell line, one PDX-derived cell line, and several isogenic cell lines with RET fusions. Using these models, we re-examined the efficacy and mechanism of action of cabozantinib and found that this RET inhibitor was effective at blocking growth of cell lines, activating caspase 3/7 and inhibiting activation of ERK and AKT. Cabozantinib treatment of mice bearing RET-fusion-positive cell line xenografts and two PDXs significantly reduced tumor proliferation without adverse toxicity. Moreover, cabozantinib was effective at reducing growth of a lung cancer PDX that was not responsive to RXDX-105. Transcriptomic analysis of lung tumors and cell lines with RET alterations showed activation of a MYC signature and this was suppressed by treatment of cell lines with cabozantinib. MYC protein levels were rapidly depleted following cabozantinib treatment. Taken together, our results demonstrate that cabozantinib is an effective agent in preclinical models harboring *RET* rearrangements with three different 5' fusion partners (*CCDC6*, *KIF5B* and *TRIM33*). Notably, we identify MYC as a protein that is upregulated by RET expression and down-regulated by cabozantinib treatment, opening up potentially new therapeutic avenues for combinatorial targeting RET-fusion driven lung cancers. The novel RET fusion-dependent preclinical models described herein represent valuable tools for further refinement of current therapies and the evaluation of novel therapeutic strategies.

## Introduction

The *rearranged during transfection (RET)* gene encodes a proto-oncogene and was identified in 1985 (Takahashi et al., 1985). The gene maps to chromosome 10q11.2 and encodes a single-pass transmembrane receptor tyrosine kinase consisting of three domains: an extracellular domain, a transmembrane domain and a tyrosine kinase domain. The primary RET ligands belong to the glial-derived neurotrophic factor (GDNF) family which activates RET by first binding to their cognate receptor (GDNF receptor alpha) and then the GDNF-GRF $\alpha$  complex dimerizes with RET, leading to its autophosphorylation and activation. The phospho-tyrosine residues on RET serve as docking sites for the SH2 domains of several signaling molecules that activate downstream pathways (e.g. RAS/MAPK, PI3K/AKT) associated with cellular proliferation, migration, and differentiation (Arighi et al., 2005; Phay and Shah, 2010).

Rearrangement of the RET gene via inter- or intra-chromosomal translocation where the kinase domain of *RET* is fused to another gene results in a fusion oncogene (Stransky et al., 2014). A fusion of the kinase domain of *RET* with the 5' region of *CCDC6* was initially discovered in papillary thyroid carcinoma (Fusco et al., 1987) and subsequently, *RET* fusions with various other upstream partners were discovered in lung (Li et al., 2017; Lipson et al., 2012; Suehara et al., 2012; Takeuchi et al., 2012) and other cancers (Le Rolle et al., 2015; Paratala et al., 2018). In non-small cell lung carcinoma (NSCLC), *RET* fusions have been described with at least twelve 5' partner genes including *KIF5B*, *CCDC6*, *NCOA4*, *MYO5C*, *EPFA5*, *TRIM33*, *CLIP1*, *ERC1*, *PICALM*, *FRMD4A*, *RUFY2* and *TRIM24* (Ferrara et al., 2018). The N-terminal partner of RET in all fusion variants described to date contributes a protein-protein interaction domain (e.g. coiled coil domain) that aid in dimerization of the fusion oncoprotein, allowing for constitutive RET activation by autophosphorylation (Ju et al., 2012). The tumorigenic potential of *RET* fusion proteins has been demonstrated *in vitro* and *in vivo* (Li et al., 2017; Takeuchi et al., 2012). In addition to gene rearrangements, RET can also be activated by kinase domain mutations in medullary thyroid carcinoma (Jhiang, 2000).

Oncogenic RET is an actionable therapeutic target that is found in 1-2% of NSCLC and 9% of thyroid cancers (Elisei et al., 2013; Zehir et al., 2017). In NSCLC, several small molecule RET inhibitors that fall into the categories of multi-kinase inhibitors (e.g. cabozantinib (Drilon et al., 2016), sunitinib (Gautschi et al., 2017), lenvatinib (Gautschi et al., 2017), vandetanib (Yoh et al., 2017), RXDX-105 (Drilon et al., 2019a)) or selective inhibitors such as selpercatinib (LOXO-292) (Drilon et al., 2019b; Drilon et al., 2020) and pralsetinib (BLU-667) (Gainor et al., 2019), have been tested in single patients or clinical trials. However, the activity of multi-kinase inhibitors including cabozantinib, RXDX-105, vandetanib, and sunitinib in patients with *RET*-rearranged NSCLC (overall response rate (ORR): 18%-37%; median progression-free survival (PFS): 2.3-5.5 months) (Drilon et al., 2016; Gautschi et al., 2017) is clearly inferior to the responses and survival outcomes seen with selective TKIs in other driver oncogenes, such as *EGFR* mutations (ORR 56%-85% and median PFS 9.2-13.7 months) (Castellanos et al., 2017), *ALK* (ORR 60%-95% and median PFS 8-11 months) (Caccese et al., 2016), and *ROS1* (ORR 65%-85% and median PFS 9.1-19.3 months) rearrangements (Facchinetti et al., 2017). In the case of RXDX-105, tumors arising from *KIF5B-RET* fusions (0/20) did not respond to the drug whereas patients with non-*KIF5B-RET* fusions showed an ORR of 67% (6/9) in phase I/1B clinical trial (Drilon et al., 2019a), further raising concerns about the ability of multi-kinase inhibitors to inhibit only select RET fusions. In addition, multi-kinase inhibitors such as cabozantinib are often associated with a high rate of drug-related toxicities, leading to dose reduction in up to 70% of patients (Drilon et al., 2016). Selective inhibition of RET has shown more promise in lung cancer. In a phase 1 trial of pralsetinib (BLU-667), the ORR was 58% in *RET* fusion-positive NSCLC (Gainor et al., 2019). Similarly, selpercatinib has shown an ORR of 64% in *RET* fusion-positive NSCLC patients who were previously treated with therapy and an ORR of

85% in patients that received no previous RET therapy (Drilon et al., 2019b; Drilon et al., 2020; Wirth et al., 2019).

There is no comprehensive study of the efficacy of any RET inhibitor in preclinical lung cancer models with *RET* fusions (Drilon et al., 2019b; Drilon et al., 2020; Gainor et al., 2019). Indeed, the efficacy of cabozantinib, selpercatinib and pralsetinib has only been reported in one patient-derived lung cancer cell line, LC-2/ad (Li et al., 2017) likely due to the paucity of patient-derived disease models. In this study we developed four new patient-derived lung cancer models with different RET fusions and examined the efficacy of cabozantinib in these models. We further analyzed TCGA data sets to examine the signaling pathways that are activated in lung cancers with *RET* rearrangements with multiple upstream fusion partners. We report that cabozantinib effectively inhibited growth of *RET*-rearranged cell lines harboring oncogenic *CCDC6-RET*, *TRIM33-RET* and *KIF5B-RET* fusions and was effective *in vivo* in patient-derived xenografts. Importantly, cabozantinib was effective in a *KIF5B-RET* model that did not respond to RXDX-105. We found that the *MYC* pathway is activated by *RET* fusions and *MYC* expression is decreased by cabozantinib treatment, suggesting that combination therapy of RET and novel *MYC* inhibitors could potentially improve patient outcomes.

## Results

### Generation and characterization of novel *RET*-rearranged cell lines

To perform preclinical investigation of RET inhibitors, we compiled a collection of *RET*-driven cell lines. This collection included the previously reported LC-2/ad cell line (harboring a *CCDC6-RET* fusion) (Li et al., 2017) as well as two novel patient-derived (ECLC5B harboring *TRIM33-RET*) and PDX-derived (LUAD-0002 harboring *KIF5B-RET*) cell lines that we generated. The patient demographic details and genomic profiling of the novel models by the MSK-IMPACT platform is given in **Supplementary Table 1** and **Supplementary Table 2**, respectively. Additionally, we have established isogenic cell lines by overexpressing the *CCDC6-RET* fusion in 3T3 murine fibroblasts (NIH-3T3) and immortalized human broncho-epithelial cells (HBECp-RET1). We first examined expression of the respective *RET* fusion mRNA by PCR using primers that bind to 5' partners and exon 12 of *RET*, respectively, (**Figure 1A**). Protein expression and phosphorylation were confirmed by Western blotting (**Figure 1B**). There were multiple bands in lysates extracted from some cell lines that were identified by the total and anti-RETpY905 antibody possibly representing different isoforms (in the case of the patient-derived and PDX-derived cell lines) or post-translational modifications (**Figure 1B**).

### Cabozantinib inhibits growth and induces apoptosis in cell lines harboring RET fusions

We next evaluated the effect of cabozantinib on growth of RET fusion-positive or control cells. As comparison we used two other multi-kinase inhibitors (vandetanib, RXDX-105) that have been shown to inhibit RET (Gautschi et al., 2017, Drilon et al., 2019a). While the non-tumor HBECp cell line displayed only marginal sensitivity to the 3 compounds, growth of RET-driven cell lines was reduced at low nanomolar concentrations by the three RET inhibitors (**Figure 1C and D**). ECLC5B cells (*TRIM33-RET*) were the most responsive to cabozantinib and RXDX-105. Growth of all RET-fusion driven cell lines were inhibited by vandetanib with similar  $IC_{50s}$ . We further assessed the ability of these compounds to activate caspase 3/7 as a surrogate for apoptosis. Treatment of cells with cabozantinib for 48 h resulted in a small but significant dose-dependent activation of caspase 3/7 in the three cell lines tested (**Figure 1E**). Similarly, vandetanib and RXDX-105 also stimulated caspase 3/7 in a dose-dependent manner (**Figure 1E**).

## Signaling pathways activated by RET activation

To identify cell signaling pathways activated by RET, we performed phospho-kinome profiling of 43 kinases involved in RTK-induced signaling in HBECp and RET-transformed, HBECp-RET1 cells. Expression of CCDC6-RET caused significant increases in phosphorylation of ERK, RSK, AKT, JNK, STAT3, STAT5B and GSK3 (**Figure 2A**). Three main signaling axes were identified in down-regulated phospho-proteins, namely, CHK2-TP53, PRAS40-MTOR, and SRC family kinases (**Figure 2B**). Additionally, phosphorylation of JUN and total beta-catenin level were significantly decreased in cells expressing the CCDC6-RET fusion protein (**Figure 2A and B**).

We further treated HBECp-RET1 cells with cabozantinib to evaluate its effect on phospho-proteome changes induced by RET overexpression. Remarkably, cabozantinib significantly decreased phosphorylation of all proteins that were significantly phosphorylated by RET expression, restored phosphorylation of the CHK2-p53 axis, SRC and JUN, and expression of beta-catenin (**Figure 2C**). Phosphorylation levels of PRAS40 and MTOR were also upregulated after treatment with cabozantinib, although these changes did not reach statistical significance. These findings were largely confirmed in LUAD-0002AS1 cells harboring a *KIF5B-RET* fusion, where cabozantinib treatment resulted in decreased phosphorylation of ERK, AKT, JNK, STAT2, STAT5 and STAT6 (**Figure 2D**). Interestingly, phosphorylation of SRC family kinases (SRC, YES, LCK) was decreased in LUAD-0002AS1 cells after cabozantinib treatment, consistent with previous reports of prominent src activation in a *Drosophila* model of *KIF5B-RET* fusion (Das and Cagan, 2017). Of note, phosphorylation of PRAS40, MTOR, AMPK $\alpha$  and CHK2 was also decreased after cabozantinib treatment, suggesting that additional differences beyond those previously reported (Das and Cagan, 2017) exist between different *RET* fusions (**Figure 2D**). We confirmed our findings of AKT and ERK inhibition by Western blot analysis in HBECp-RET1, LC-2/ad and ECLC5B cells (**Figure 2E**).

## *RET*-driven lung tumors demonstrate MYC transcriptional signatures that are inhibited with cabozantinib treatment

To identify transcriptomic changes associated with *RET* expression, we analyzed TCGA lung adenocarcinoma RNA sequencing data. We identified 3 cases (2 *RET* fusions, 1 activating point mutation) and compared their transcriptomes to healthy lung tissues. Exploratory data analysis indicated that *RET*-driven tumors segregated from normal lung tissue as expected (data not shown). The output of differential gene expression analysis was ranked and subsequently gene set enrichment analysis was performed. We identified significant activation of MYC-associated transcriptional signatures (**Figure 3A**). The full results of differential expression analysis and GSEA analysis for *RET*-driven LUAD are summarized in **Supplementary Tables 3 and 4**, respectively.

To investigate the effect of cabozantinib on *RET* fusion-associated gene expression, we treated the ECLC5B cell line, which was the most sensitive cabozantinib, for three hours and performed gene expression analysis. **Figure 3B** demonstrates principal component analysis indicating different grouping of untreated and cabozantinib-treated samples and **Supplementary Figure 1** demonstrates a summary heatmap of the differential expression analysis. Remarkably, *MYC* oncogene was in the top 5 of most downregulated genes, accompanied by many associated transcriptional targets (**Figure 3C**). GSEA analysis demonstrated that *RET*-associated MYC transcriptional signatures were significantly downregulated by cabozantinib (**Figure 3D**). Furthermore, Western blotting analysis using

two anti-MYC polyclonal antibodies targeting independent epitopes revealed a rapid and significant decline in MYC expression following cabozantinib treatment (0.1  $\mu$ M), plateauing at the 1 h time point (**Figure 3E and F**). The rapid decrease in MYC level (half-time: <30 minutes) suggests that expression of MYC requires continuous input from activated RET. The full results of differential expression analysis and GSEA analysis for ECLC5B cells treated with cabozantinib are summarized in **Supplementary Tables 5 and 6**, respectively.

We further performed overlapping analysis of the two expression datasets to determine genes that were significantly upregulated (adjusted p value <0.05) in RET-driven LUAD and downregulated after cabozantinib treatment. We identified multiple genes with oncogenic properties such as *POLD2* (DNA polymerase delta 2 participating in DNA replication), *MCM5* (Minichromosome Maintenance Complex Component 5 involved in the initiation of DNA replication), *NGF* (nerve growth factor), *TUBA4A* (tubulin alpha 4a participating in cell division), and *ETV4*, an oncogenic transcription factor previously demonstrated as critical for RET signaling (Lu et al., 2009).

### **Efficacy of cabozantinib administration on growth of RET inhibitor treatment-naive preclinical models with RET fusions**

To determine how effective cabozantinib is *in vivo*, we treated mice bearing PDX or engineered cell line xenograft tumors arising from our RET fusion-driven models with compound and assessed growth over time. Animals were treated with doses ranging from 10 mg/kg QD to 100 mg/kg QD. These doses are based on previous *in vivo* studies in mice showing that 30 mg/kg cabozantinib caused more than 50% inhibition of phosphorylation of RET fusion (Y905) and complete inhibition was observed at a dose of 60 mg/kg (Paratala et al., 2018). The tumor volume (left panel), area under curve analysis to compare response over the entire time of treatment (middle panel) and the size of individual tumors at the end of the study (right panel) of each tumor are shown in **Figure 4A**. Treatment of mice bearing LUAD-0002AS1 PDX tumors (KIF5B-RET) resulted in a significant reduction in growth following administration of 10 mg/kg QD ( $p=0.001$ , 40% difference between vehicle and treatment) or 50 mg/kg QD ( $p<0.0001$ , 85% difference between vehicle and treatment) cabozantinib compared to the vehicle-treated group at the end of the study (**Figure 4A, left panel**). In both treatment groups, tumor growth was significantly reduced in response to cabozantinib administration (**Figure 4A, middle panel**), with all tumors showing reduction in growth (**Figure 4A, right panel**). Treatment with 50 mg/kg cabozantinib resulted in complete inhibition of growth. Administration of cabozantinib did not affect animal weight (**Figure 4A, inset**). We next determined the efficacy of cabozantinib on the growth of tumors arising from isogenic HBEC and NIH-3T3 cell lines expressing a CCDC6-RET fusion. The tumor volume (left panel), area under curve analysis to compare response over the entire time of treatment (middle panel) and the size of individual tumors at the end of the study (right panel) of each tumor are shown in **Figure 4B and C**. As observed with the KIF5B-RET-positive PDX models, cabozantinib caused significant reductions in tumor growth at the doses tested in the two models (**Figure 4B and C**). Cabozantinib treatment blocked tumor growth completely for the first 10 and 15 days, respectively, for the NIH-3T3-CCDC6/RET and HBECp-RET1 models. However, NIH-3T3-CCDC6/RET and HBECp-RET1 xenograft tumors started to regrow towards the end of the treatment periods (**Figure B and C, left panel**). We did not observe any statistically significant reduction in animal weight in any of the cabozantinib treatment groups (**Figure 4B and C, inset, left panel**).

### Efficacy of cabozantinib on the growth of an RXDX-105-resistant PDX model

To expand these efficacy studies, we examined the effect of cabozantinib on growth of PDX tumors (LUAD-0046AS1) that were derived from a patient who did not respond to RXDX-105. Tumor-bearing mice were treated with vehicle, cabozantinib (30 mg/kg QD) or RXDX-105 (30 mg/kg BID). As expected, treatment with RXDX-105 did not significantly affect growth of LUAD-0046AS1 PDX tumors (KIF5B-RET) (vehicle:  $912.3 \pm 213.1 \text{ mm}^3$ ; RXDX-105:  $853.2 \pm 84.7 \text{ mm}^3$ ) (**Figure 4D**). However, treatment with cabozantinib blocked growth of LUAD-0046AS1 PDX tumors completely (starting volume:  $133.8 \pm 2.3 \text{ mm}^3$ ; end volume:  $139 \pm 9.6 \text{ mm}^3$ ). This dosage of RXDX-105 was previously shown to reduce growth of RET fusion-driven cell lines xenograft tumors (Li et al., 2017). All tumors in the cabozantinib treatment group responded to the drug (**Figure 4D, right panel**). There was no significant reduction in animal weight in any of the treatment arms (**Figure 4D, left panel, inset**).

### Discussion

Due to a lack of preclinical models of lung cancer with *RET* rearrangements there has been very few studies examining the efficacy of RET inhibitors and signaling pathways exploited by RET fusions to drive tumorigenesis prior to clinical trials. Here we generated four novel preclinical patient-derived models of RET-rearranged lung cancers and used these models to examine the efficacy of the RET multi-kinase inhibitor cabozantinib in these patient-derived and isogenic models. In addition, we sought to identify the biochemical pathways that are recruited to drive RET fusion-dependent growth in these models.

We found that cabozantinib was effective *in vitro* and *in vivo* in models with three different 5' *RET* fusion partners, including two models harboring *KIF5B-RET* fusion, which was previously shown to respond poorly to RXDX-105 (Drilon et al., 2019a). Cabozantinib inhibited growth of several cell lines and animal models with RET fusions. Of note, cabozantinib was effective in a *KIF5B-RET* PDX model derived from a patient tissue that did not respond to RXDX-105. Our profiling of RET-associated phospho-proteome signaling in isogenic cell lines harboring a *CCDC6-RET* fusion demonstrated activation of ERK, AKT, STAT and suppression of CHK2 and P53; treatment with cabozantinib reversed these changes. While most of our findings were confirmed in a PDX-derived cell line harboring a *KIF5B-RET* fusion, a peculiar discrepancy occurred in the response of SRC family kinases where inhibition was only seen in cells harboring *KIF5B-RET* fusion, while upregulated in the case of *CCDC6-RET*. This finding is congruent with previously demonstrated ability of *KIF5B-RET* fusion to induce SRC and EGFR/FGFR activation (Das and Cagan, 2017). Accordingly, a phase 1/2 clinical study of TPX-0046 (NCT04161391), a multi-targeted RET and SRC kinase inhibitor, is ongoing for TKI-naïve and -pretreated patients with RET-altered lung, thyroid and other cancers (Drilon et al., 2019c).

To gain insight into how RET fusions may activate growth we used transcriptomic profiling of RET-driven lung adenocarcinomas which highlighted an enhanced *MYC* signature in these tumors. Correspondingly, cabozantinib treatment of a *RET*-fusion positive cell line led to *MYC* oncogene downregulation, suppression of the *MYC* signature and lower *MYC* protein expression. These results indicate that RET inhibitors can regulate *MYC* expression at the transcriptional level. Although it is possible that there is also enhanced *MYC* protein degradation, our study did not specifically address this. Alterations in *MYC* signaling are hallmarks of many human cancers, such as small cell lung cancer and Burkitt's lymphoma (Dalla-Favera et al., 1982; Kim et al., 2016), and alterations in the *MYC* pathway has been observed in approximately 30% of cancers with diverse histologies (Schaub et al., 2018). While this connection between the *MYC* pathway and oncogenesis is recognized, this is the

first report of a potential role for MYC in RET-induced tumorigenesis. Silencing *MYC* expression in multiple tumor models with siRNAs leads to tumor regression (Han et al., 2019; Jain et al., 2002; Shachaf and Felsher, 2005), suggesting that MYC may be exploited for therapy. Although direct pharmacological inhibition of MYC remains a challenge, recent studies have shed a promising light on targeting this potent transcription factor (Han et al., 2019). Notably, silencing MYC expression in multiple tumor models leads to tumor regression (Han et al., 2019; Jain et al., 2002; Shachaf and Felsher, 2005). Our finding that MYC expression requires continued signaling from RET opens a potentially new avenue for combinatorial targeting of RET-fusion driven lung cancers with RET and new MYC inhibitors to improve response rates.

As mutational activation of downstream signaling mediators is a demonstrated mechanism of resistance to RTK inhibitors, it is important to map RET-associated signaling pathways to properly investigate and predict mechanisms of resistance and identify opportunities for therapeutic strategies to overcome this resistance. We used four novel patient-derived preclinical models to begin to map RET fusion-associated signaling. These models will be invaluable in future testing of new therapy and to develop models of RET-inhibitor resistance *in vitro* and *in vivo* to profile drug resistance mechanisms.

## Materials and methods

**Compound and cell lines.** The human lung adenocarcinoma cell line LC-2/ad (Cat. No. 94072247) was obtained from Riken Cell Bank (Japan). The HBECp-RET1 cell line was generated by expressing CCDC6-RET and a dominant-negative p53 (c-terminal region of wild-type p53) (Sasai et al., 2011) in HBEC3-KT cells (human bronchial epithelial cells immortalized by CDK4 and TERT overexpression) (Sato et al., 2006) and was described previously (Li et al., 2017). All cell lines were tested every 6 months for mycoplasma and *RET* fusion verified by PCR each time a new frozen vial of stock was thawed. Novel cell lines and PDXs were verified by MSK-IMPACT NGS testing. All primary antibodies used in the present study were obtained from Cell Signaling Technology (Danvers, MA) and were validated by the manufacturer. Antibodies against phospho-RET (Y905; #3221), RET (#3220), phospho-ERK (T202/Y204; #9101), ERK (#4695), phospho-AKT (S473; #4060), AKT (#4691), GAPDH (#5174), and MYC (D3N8F, #13987, targets the central region and D84C12, #5605, targets the amino terminal region) were all used at 1:1000 dilution. All cell culture growth media (except for keratinocyte serum-free medium), antibiotics and phosphate-buffered saline (PBS) were prepared by the MSK Media Preparation Core Facility. Fetal bovine serum (FBS), proteome profiling arrays and secondary antibodies conjugated to horseradish peroxidase (HRP) were procured from R and D Systems (Minneapolis, MN). RXDX-105 (agerafenib, CEP32496), cabozantinib, lenvatinib, vandetanib, and ponatinib were purchased from Selleckchem (Houston, TX). Promega's ApoOne Homogenous Caspase 3/7 activity assay kit, AlamarBlue viability dye, keratinocyte serum-free medium (KSM), tissue culture plastic wares, NuPAGE gels, blotting buffers and all Western blotting reagents were obtained from ThermoFisher Scientific (Waltham, MA). Protease and phosphatase inhibitor cocktails, RIPA lysis buffer (10X) and all other chemicals not listed above were purchased from EMD-Millipore Sigma (St. Louis, MO). All oligonucleotides used for PCR assays were obtained from Integrated DNA technologies (Coralville, IA).

**Growth and propagation of cell lines.** All cell lines were grown in a humidified incubator with 5% CO<sub>2</sub> at 37 °C. Cells were maintained in 75-cm<sup>2</sup> flasks and subcultured when approaching 75% confluence using 0.25% trypsin/1 mM EDTA solution. ECLC5B cells were maintained in DME:F12 medium supplemented with 10% (vol/vol) FBS and 1% (vol/vol) antibiotic solution. LC-2/ad and HBECp-RET1 cells were maintained in RPMI-1640 medium supplemented with 10% (vol/vol) FBS and 1% (vol/vol) antibiotic solution. HBEC3-KT cells

were maintained in keratinocyte serum-free media supplemented with 50 µg/mL bovine pituitary extract (BPE) and 5 ng/mL recombinant epidermal growth factor (EGF).

**Generation of cell lines and patient-derived xenografts.** Tissue samples were collected under an MSK institutional IRB-approved biospecimen collection protocol and all patients provided informed consent for collection and use of tissues. Animals were monitored daily and cared for in accordance with guidelines approved by the Memorial Sloan Kettering Cancer Center Institutional Animal Care and Use Committee and Research Animal Resource Center. To obtain pleura effusion a thoracentesis was performed on a patient with acquired resistance to cabozantinib and samples were collected in a sterile container in which heparin was added (10 USP units/mL fluid). Epithelial cells were isolated by differential centrifugation on Ficoll gradient. To obtain a single cell suspension, cells were treated with trypsin, neutralized with DMEM/F12 medium supplemented with 10% FBS, filtered through a 40 µm cell strainer, pelleted and re-suspended in DMEM/F12 medium with 10% FBS. The cabozantinib-resistant cell line was considered established after 20 continuous passages and named ECLC5. Given the rarity of RET-inhibitor sensitive cell lines with confirmed RET fusions, we sought to establish a subline with enhanced sensitivity to cabozantinib. A previous study has shown that TKI sensitivity can be restored to drug-resistant tumor cells in culture by withdrawing the selection pressure (cabozantinib in our case) (Chmielecki et al., 2011). We therefore, cultured ECLC5 long-term in the absence of cabozantinib in order to allow any drug-responsive subclones of cells to gain a proliferative advantage. This cabozantinib-sensitive subpopulation was named ECLC5B and this was used for experiments in this study. Patient-derived xenograft models were generated by implanting biopsied lung tumor samples (minced and then mixed with 50% (vol/vol) matrigel) in the subcutaneous flank of female NOD/SCID gamma (NSG) mice (Jackson Laboratory, Bar Harbor, ME). PDX tumors were transplanted for at least 3 serial passages before the model was considered established and used for efficacy studies. The LUAD-0046AS1 PDX model was created from tissue obtained from a patient who was treated with RXDX-105 but did not respond. The LUAD-0002AS1 PDX model was derived from a patient who never received any RET therapy. The LUAD-0002AS1 cell line was created from the 4<sup>th</sup> passage PDX tissue. Briefly, fresh tumors were cut into small pieces and then digested in a cocktail of tumor dissociation enzymes obtained from Miltenyl Biotec (130-095-929) in 5 mL serum-free DME:F12 media for one hour, 37°C, with vortexing every 5-10 min, according to manufacturer's instructions. Digested samples were resuspended in 45 mL complete growth media to inactivate the dissociation enzymes and then cells pelleted by centrifugation. Finally, cells were plated in complete growth media and allowed to propagate over multiple generations, trypsinized when necessary to subculture and eventually only single cells remained. The cell line was considered established after 20 continuous passages.

**Genomic characterization.** Cell lines and PDX were profiled by the MSK-IMPACT (Integrated Mutation Profiling of Actionable Cancer Targets) platform, which is a large panel sequencing (NGS) assay, that was used here to detect mutations and copy-number alterations involving up to 468 cancer-associated genes (Cheng et al., 2015). As the corresponding patient-matched normal DNA was unavailable, single nucleotide variants (SNVs) representing known COSMIC somatic mutations or truncating mutations in tumor suppressor genes and copy number variants (CNVs) were tabulated.

**Efficacy studies in xenograft models.** For efficacy studies, xenograft tumor samples were cleaned and then minced, mixed with matrigel and implanted into a subcutaneous flank of female NSG mice to generate xenografts. Tumor-bearing animals were randomized to groups of 5 when tumors reached approximately 100 mm<sup>3</sup> volume so that averages of tumor volume within and between groups were similar. Treatment was initiated with vehicle,

cabozantinib (10 mg/kg QD, 25 mg/kg QD, 30 mg/kg QD, 50 mg/kg QD or 100 mg/kg QD) or RXDX-105 (30 mg/kg BID). Cabozantinib was reconstituted in a vehicle consisting of 30% polypropylene glycol, 5% Tween-80 and 65% D5W (dextrose 5% water) and RXDX-105 was resuspended in 15% captisol. Both compounds were administered by oral gavage. Tumor size and body weight were measured twice weekly and tumor volume was calculated using the formula: length x width<sup>2</sup> x 0.52.

**Cell growth, drug treatment, viability and caspase 3/7 activity assays.** Cells were plated directly into chemicals at a density of 6,000 (viability) or 20,000 (caspase 3/7 activity) cells per well in white, clear bottom 96-well plates. Viability was assayed after 96 h of treatment using AlamarBlue viability dye and the fluorescence (Ex: 530 nm, Em: 570 nm) was measured using a Spectramax M2 microplate reader (Molecular Devices, Sunny Vale, CA). Data was analyzed by non-linear regression using Graphpad Prism v8.0 to obtain IC<sub>50</sub> values. Caspase 3/7 enzymatic assay was performed 48 h after treatments using the ApoOne homogeneous caspase 3/7 activity kit according to manufacturer's instruction. Each condition was assayed in triplicate determinations in at least 2 experiments. For Western blotting studies, cells were plated at a density of 1 million cells per well of 6 well plates and used 4 days later. Cells were deprived of serum for 24 h prior to treatment for Western blotting studies, and all treatments were conducted in serum-free medium.

**Isolation of RNA, cDNA synthesis and RT-PCR.** For detection of the *RET* fusion transcript in cell lines and PDX tissues, total RNA were extracted using a Qiagen RNA mini kit and cDNAs were synthesized using SuperScript IV VILO (ThermoFisher) according to the manufacturer's instructions. The following primers were used for RT-PCR: ***GAPDH Fw*** 5'-GGC GCT GAG TAC GTC GTG GAG TCC-3', ***GAPDH Rv*** 5'-AAA GTT GTC ATG GAT GAC CTT GG-3', ***CCDC6 exon 1 Fw*** 5'-GCA TTG TCA TCT CGC CGT TCC G-3', ***KIF5B exon 15 Fw*** 5'-GCA ACT TTA GCG AGT ATA GAT-3', ***TRIM33 exon 14 Fw*** 5'-AGC AAG AAC CTG GGA CTG AAG ATG 3', ***RET exon 12 Rv*** 5'-TGC TCT GCC TTT CAG ATG GAA GG-3'.

**Preparation of whole-cell extracts and Western blotting.** Cells were lysed in 350 µL RIPA lysis buffer that was supplemented with 1 mM sodium orthovanadate, 1 mM DTT (dithiothreitol) and protease and phosphatase inhibitor cocktails according to the manufacture's instructions. Lysates were denatured in 2X Laemmli sample buffer at 55 °C for 5 min, resolved on 4-12% NuPAGE reducing gels and transferred onto PVDF (polyvinylidene fluoride) membranes. Membranes were blocked in 3% BSA in TBST buffer (tris-buffered saline with 0.1% Tween-20) for 1 h at room temperature and probed with primary antibodies overnight. Bound antibodies were detected with peroxidase-labeled goat anti-mouse or goat anti-rabbit IgG and developed with ECL Western blotting detection reagents. Images were captured on X-ray film. All experiments were repeated at least 2 times.

**Phospho-kinase proteomic profiling array.** We used a human Phospho-Kinase Array Kit containing duplicate validated controls and capture antibodies that simultaneously detect the relative phosphorylation state of 43 human kinases (R&D Systems), according to the manufacturer's protocol. A total of 5x10<sup>6</sup> cells were plated in 10 cm dishes and then deprived of serum for 24 h. In brief, the array membranes were blocked, incubated with 300 µg cell lysates per array overnight at 4 °C. The next day arrays were washed three times, incubated with biotinylated antibodies for 2 h at room temperature, washed three times, incubated with streptavidin-HRP for 30 min at room temperature, washed again three times and developed with ECL Western blotting detection reagents. The kinase spots were visualized with X-ray

films (Ewen-Parker X-ray). The average pixel densities of duplicate spots were determined using the ImageJ software (<http://imagej.nih.gov/ij/>).

**TCGA RNAseq expression analysis.** Gene expression data from The Cancer Genome Atlas was retrieved from the public functional genomics data repository Gene Expression Omnibus (accession GSE62944) (Rahman et al., 2015). Data were normalized and analyzed using DESeq2 package in the R programming environment. Gene Set Enrichment Analysis (GSEA) was conducted and visualized using clusterProfiler R package. Additionally, ggplot2 R package was used for data visualization.

**Gene expression microarray analysis.** ECLC5B cells were plated at a density of 500,000 cells per well in 6-well plates and then treated 24 h later with 0.1  $\mu$ M cabozantinib or 0.1% DMSO in triplicates. After 3 h, cells were washed with ice-cold PBS and total RNA was extracted using RNeasy mini kit (Qiagen, Germantown, MD). All microarray hybridization and scanning steps were performed by the MSK Integrated Genomics Operations Core Laboratory. Briefly, total RNA was converted to double-strand cDNA with oligo d(T) primers and reverse transcriptase before *in vitro* transcription with biotinylated UTP and CTP. The resulting biotinylated cRNA was then fragmented and hybridized for 16 h at 45°C to the Affymetrix oligonucleotide Human HG-U133A Genechip (Santa Clara, CA), containing 22,215 probe sets representing ~18,500 transcripts and 14,500 genes. The resulting data were analyzed using R programming environment. First, data was Robust Multichip Average (RMA)-normalized and unsupervised clustering profiling was performed using Principal Component Analysis. One outlier sample was identified in the untreated group and removed from further analysis. Linear regression analysis was performed using limma R package (<https://www.rdocumentation.org/packages/limma/versions/3.28.14>) to detect differentially expressed genes. Gene Set Enrichment Analysis (GSEA) was conducted and visualized using clusterProfiler R package (<https://www.rdocumentation.org/packages/clusterProfiler/versions/3.0.4>).

**Statistical analysis.** Student's t-test was used to compare caspase activity or protein phosphorylation. For animal studies, area under curve (AUC) analysis was used to compare the average tumor volume between groups. Briefly, area under curve values and standard errors were computed as an estimation of the surface area between baseline values (mean value of the tumor volumes at the beginning of the treatment) and growth curves for vehicle and each treatment conditions. Treatment response was compared to the vehicle group using multiple Student's t-tests. All data were plotted and analyzed using GraphPad Prism v8 software.  $P < 0.05$  was considered significant.

## Competing interests

Takuo Hayashi, Igor Odintsov, Roger S. Smith, Kota Ishizawa, Zebing Liu, Allan Jo-Weng Lui, Christopher Kurzatkowski, Huichun Tai, Shinji Kohsaka, Ken Suzawa, Morana Vojnic, Lukas Delasos, Marissa S. Mattar, Eric Gladstone, Siddharth Kunte, Inna Khodos, Monika A. Davare, Elisa De Stanchina and Emily Cheng report no potential conflict of interest.

Alexander Drilon reports consulting/advisory roles for Ignyta, Loxo Oncology, TP Therapeutics, AstraZeneca, Pfizer, Blueprint Medicines, Genentech/Roche, Helsinn Therapeutics, BeiGene, Hengrui Therapeutics, Exelixis, Bayer, Tyra Biosciences, Verastem, Takeda/Millennium, BerGenBio, MORE Health, Eli Lilly and Company, and Verastem; royalties for Pocket Oncology; honoraria from Medscape, OncoLive, PeerVoice, Physician's Education Resource, Targeted Oncology, MORE Health, Research to Practice, Foundation Medicine, and Peerview; and research funding from Foundation Medicine.

Marc Ladanyi has received advisory board compensation from Boehringer Ingelheim, AstraZeneca, Bristol-Myers Squibb, Takeda, Bayer, and Paige.AI, and research support from LOXO Oncology, Helsinn Healthcare, Elevation Oncology and Merus.

Romel Somwar has received research funding from Merus, Helsinn Healthcare, LOXO Oncology and Elevation Oncology for studies unrelated to this manuscript.

## Funding

This work was supported by a grant from the Stanley and Fiona Druckenmiller Center for Lung Cancer Research at Memorial Sloan Kettering Cancer Center, a U54 OD020355 grant from the National Institute of Health to Elisa de Stanchina and a Memorial Sloan Kettering Cancer Center Support Grant (P30 CA008748).

## Data and reagent availability

All genomic data are included in the supplementary tables. Cell lines, PDX models and plasmids can be requested by contacting the corresponding authors.

## Author contributions statement

Conception and design: Takuo Hayashi, Igor Odintsov, Roger S. Smith, Marc Ladanyi and Romel Somwar

Development of methodology: Igor Odintsov, Roger S. Smith, Inna Khodos, Elisa de Stanchina and Romel Somwar.

Acquisition of data (provided animals, acquired and managed patients, provided facilities, etc.): Takuo Hayashi, Igor Odintsov, Roger S. Smith, Kota Ishizawa, Allan J.W. Liu, Lukas Delasos, Christopher Kurzatkowski, Huichun Tai, Eric Gladstone, Morana Vojnic, Shinji Kohsaka, Ken Suzawa, Zebing Liu, Siddharth Kunte, Marissa S. Mattar, Inna Khodos, Monika A. Davare, Alexander Drilon, Emily Cheng, Elisa de Stanchina, Marc Ladanyi and Romel Somwar.

Analysis and interpretation of data (e.g., statistical analysis, biostatistics, computational analysis): Takuo Hayashi, Igor Odintsov, Roger S. Smith, Kota Ishizawa, Allan J.W. Liu, Lukas Delasos, Christopher Kurzatkowski, Huichun Tai, Eric Gladstone, Morana Vojnic, Shinji Kohsaka, Ken Suzawa, Zebing Liu, Siddharth Kunte, Marissa S. Mattar, Inna Khodos, Monika A. Davare, Alexander Drilon, Emily Cheng, Elisa de Stanchina, Marc Ladanyi, Romel Somwar

Writing, review, and/or revision of the manuscript: Takuo Hayashi, Igor Odintsov, Roger S. Smith, Elisa de Stanchina, Monika A. Davare, Marc Ladanyi, Romel Somwar

Administrative, technical, or material support (i.e., reporting or organizing data, constructing databases):

Study supervision: Marc Ladanyi and Romel Somwar

## References

- Arighi, E., Borrello, M. G. and Sariola, H.** (2005). RET tyrosine kinase signaling in development and cancer. *Cytokine Growth Factor Rev* **16**, 441-67.
- Caccese, M., Ferrara, R., Pilotto, S., Carbognin, L., Grizzi, G., Calio, A., Brunelli, M., Cuppone, F., Petraglia, S., Scarpa, A. et al.** (2016). Current and developing therapies for the treatment of non-small cell lung cancer with ALK abnormalities: update and perspectives for clinical practice. *Expert Opin Pharmacother* **17**, 2253-2266.
- Castellanos, E., Feld, E. and Horn, L.** (2017). Driven by Mutations: The Predictive Value of Mutation Subtype in EGFR-Mutated Non-Small Cell Lung Cancer. *J Thorac Oncol* **12**, 612-623.
- Cheng, D. T., Mitchell, T. N., Zehir, A., Shah, R. H., Benayed, R., Syed, A., Chandramohan, R., Liu, Z. Y., Won, H. H., Scott, S. N. et al.** (2015). Memorial Sloan Kettering-Integrated Mutation Profiling of Actionable Cancer Targets (MSK-IMPACT): A Hybridization Capture-Based Next-Generation Sequencing Clinical Assay for Solid Tumor Molecular Oncology. *J Mol Diagn* **17**, 251-64.
- Chmielecki, J., Foo, J., Oxnard, G. R., Hutchinson, K., Ohashi, K., Somwar, R., Wang, L., Amato, K. R., Arcila, M., Sos, M. L., et al.** (2011). Optimization of dosing for EGFR-mutant non-small cell lung cancer with evolutionary cancer modeling. *Sci Transl Med*, **3**, 90ra59.
- Dalla-Favera, R., Bregni, M., Erikson, J., Patterson, D., Gallo, R. C. and Croce, C. M.** (1982). Human c-myc onc gene is located on the region of chromosome 8 that is translocated in Burkitt lymphoma cells. *Proc Natl Acad Sci U S A* **79**, 7824-7.
- Das, T. K. and Cagan, R. L.** (2017). KIF5B-RET Oncoprotein Signals through a Multi-kinase Signaling Hub. *Cell Rep* **20**, 2368-2383.
- Drilon, A., Fu, S., Patel, M. R., Fakih, M., Wang, D., Olszanski, A. J., Morgensztern, D., Liu, S. V., Cho, B. C., Bazhenova, L. et al.** (2019a). A Phase I/Ib Trial of the VEGFR-Sparing Multikinase RET Inhibitor RXDX-105. *Cancer Discov* **9**, 384-395.
- Drilon, A., Oxnard, G., Wirth, L., Besse, B., Gautschi, O., Tan, S. W. D., Loong, H., Bauer, T., Kim, Y. J., Horiike, A. et al.** (2019b). Registrational Results of LIBRETTO-001: A Phase 1/2 Trial of LOXO-292 in Patients with RET Fusion-Positive Lung Cancers. *Journal of Thoracic Oncology* **14**, S6-S7.
- Drilon, A., Oxnard, G. R., Tan, D. S. W., Loong, H. H. F., Johnson, M., Gainor, J., McCoach, C. E., Gautschi, O., Besse, B., Cho, B. C. et al.** (2020). Efficacy of Selpercatinib in RET Fusion-Positive Non-Small-Cell Lung Cancer. *N Engl J Med* **383**, 813-824.
- Drilon, A., Rekhman, N., Arcila, M., Wang, L., Ni, A., Albano, M., Van Voorthuysen, M., Somwar, R., Smith, R. S., Montecalvo, J. et al.** (2016). Cabozantinib in patients with advanced RET-rearranged non-small-cell lung cancer: an open-label, single-centre, phase 2, single-arm trial. *Lancet Oncol* **17**, 1653-1660.
- Drilon, A., Rogers, E., Zhai, D., Deng, W., Zhang, X., Lee, D., Ung, J., Whitten, J., Zhang, H., Liu, J. et al.** (2019c). TPX-0046 is a novel and potent RET/SRC inhibitor for RET-driven cancers. *Annals of Oncology* **30**, 190-+.
- Elisei, R., Schlumberger, M. J., Muller, S. P., Schoffski, P., Brose, M. S., Shah, M. H., Licitra, L., Jarzab, B., Medvedev, V., Kreissl, M. C. et al.** (2013). Cabozantinib in progressive medullary thyroid cancer. *J Clin Oncol* **31**, 3639-46.
- Facchinetti, F., Rossi, G., Bria, E., Soria, J. C., Besse, B., Minari, R., Friboulet, L. and Tiseo, M.** (2017). Oncogene addiction in non-small cell lung cancer: Focus on ROS1 inhibition. *Cancer Treat Rev* **55**, 83-95.
- Ferrara, R., Auger, N., Auclin, E. and Besse, B.** (2018). Clinical and Translational Implications of RET Rearrangements in Non-Small Cell Lung Cancer. *J Thorac Oncol* **13**, 27-45.
- Fusco, A., Grieco, M., Santoro, M., Berlingieri, M. T., Pilotti, S., Pierotti, M. A., Della Porta, G. and Vecchio, G.** (1987). A new oncogene in human thyroid papillary carcinomas and their lymph-nodal metastases. *Nature* **328**, 170-2.

**Gainor, J. F., Lee, D. H., Curigliano, G., Doebele, R. C., Kim, D. W., Baik, C. S., Tan, D. S. W., Lopes, G., Gadgeel, S. M., Cassier, P. A. et al.** (2019). Clinical activity and tolerability of BLU-667, a highly potent and selective RET inhibitor, in patients (pts) with advanced RET-fusion plus non-small cell lung cancer (NSCLC). *Journal of Clinical Oncology* **37**.

**Gautschi, O., Milia, J., Filleron, T., Wolf, J., Carbone, D. P., Owen, D., Camidge, R., Narayanan, V., Doebele, R. C., Besse, B. et al.** (2017). Targeting RET in Patients With RET-Rearranged Lung Cancers: Results From the Global, Multicenter RET Registry. *J Clin Oncol* **35**, 1403-1410.

**Han, H., Jain, A. D., Truica, M. I., Izquierdo-Ferrer, J., Anker, J. F., Lysy, B., Sagar, V., Luan, Y., Chalmers, Z. R., Unno, K. et al.** (2019). Small-Molecule MYC Inhibitors Suppress Tumor Growth and Enhance Immunotherapy. *Cancer Cell* **36**, 483-497 e15.

**Jain, M., Arvanitis, C., Chu, K., Dewey, W., Leonhardt, E., Trinh, M., Sundberg, C. D., Bishop, J. M. and Felsher, D. W.** (2002). Sustained loss of a neoplastic phenotype by brief inactivation of MYC. *Science* **297**, 102-4.

**Jiang, S. M.** (2000). The RET proto-oncogene in human cancers. *Oncogene* **19**, 5590-7.

**Ju, Y. S., Lee, W. C., Shin, J. Y., Lee, S., Bleazard, T., Won, J. K., Kim, Y. T., Kim, J. I., Kang, J. H. and Seo, J. S.** (2012). A transforming KIF5B and RET gene fusion in lung adenocarcinoma revealed from whole-genome and transcriptome sequencing. *Genome Res* **22**, 436-45.

**Kim, D. W., Wu, N., Kim, Y. C., Cheng, P. F., Basom, R., Kim, D., Dunn, C. T., Lee, A. Y., Kim, K., Lee, C. S. et al.** (2016). Genetic requirement for Mycl and efficacy of RNA Pol I inhibition in mouse models of small cell lung cancer. *Genes Dev* **30**, 1289-99.

**Le Rolle, A. F., Klempner, S. J., Garrett, C. R., Seery, T., Sanford, E. M., Balasubramanian, S., Ross, J. S., Stephens, P. J., Miller, V. A., Ali, S. M. et al.** (2015). Identification and characterization of RET fusions in advanced colorectal cancer. *Oncotarget* **6**, 28929-37.

**Li, G. G., Somwar, R., Joseph, J., Smith, R. S., Hayashi, T., Martin, L., Franovic, A., Schairer, A., Martin, E., Riely, G. J. et al.** (2017). Antitumor Activity of RXDX-105 in Multiple Cancer Types with RET Rearrangements or Mutations. *Clin Cancer Res* **23**, 2981-2990.

**Lipson, D., Capelletti, M., Yelensky, R., Otto, G., Parker, A., Jarosz, M., Curran, J. A., Balasubramanian, S., Bloom, T., Brennan, K. W. et al.** (2012). Identification of new ALK and RET gene fusions from colorectal and lung cancer biopsies. *Nat Med* **18**, 382-4.

**Lu, B. C., Cebrian, C., Chi, X., Kuure, S., Kuo, R., Bates, C. M., Arber, S., Hassell, J., MacNeil, L., Hoshi, M. et al.** (2009). Etv4 and Etv5 are required downstream of GDNF and Ret for kidney branching morphogenesis. *Nat Genet* **41**, 1295-302.

**Paratala, B. S., Chung, J. H., Williams, C. B., Yilmazel, B., Petrosky, W., Williams, K., Schrock, A. B., Gay, L. M., Lee, E., Dolfi, S. C. et al.** (2018). RET rearrangements are actionable alterations in breast cancer. *Nat Commun* **9**, 4821.

**Phay, J. E. and Shah, M. H.** (2010). Targeting RET receptor tyrosine kinase activation in cancer. *Clin Cancer Res* **16**, 5936-41.

**Rahman, M., Jackson, L. K., Johnson, W. E., Li, D. Y., Bild, A. H. and Piccolo, S. R.** (2015). Alternative preprocessing of RNA-Sequencing data in The Cancer Genome Atlas leads to improved analysis results. *Bioinformatics* **31**, 3666-72.

**Sasai, K., Sukezane, T., Yanagita, E., Nakagawa, H., Hotta, A., Itoh, T. and Akagi, T.** (2011). Oncogene-mediated human lung epithelial cell transformation produces adenocarcinoma phenotypes in vivo. *Cancer Res* **71**, 2541-9.

**Sato, M., Vaughan, M. B., Girard, L., Peyton, M., Lee, W., Shames, D. S., Ramirez, R. D., Sunaga, N., Gazdar, A. F., Shay, J. W. et al.** (2006). Multiple oncogenic changes (K-RAS(V12), p53 knockdown, mutant EGFRs, p16 bypass, telomerase) are not sufficient to confer a full malignant phenotype on human bronchial epithelial cells. *Cancer Res* **66**, 2116-28.

**Schaub, F. X., Dhankani, V., Berger, A. C., Trivedi, M., Richardson, A. B., Shaw, R., Zhao, W., Zhang, X., Ventura, A., Liu, Y. et al.** (2018). Pan-cancer Alterations of the MYC Oncogene and Its Proximal Network across the Cancer Genome Atlas. *Cell Syst* **6**, 282-300 e2.

**Shachaf, C. M. and Felsher, D. W.** (2005). Tumor dormancy and MYC inactivation: pushing cancer to the brink of normalcy. *Cancer Res* **65**, 4471-4.

**Stransky, N., Cerami, E., Schalm, S., Kim, J. L. and Lengauer, C.** (2014). The landscape of kinase fusions in cancer. *Nat Commun* **5**, 4846.

**Suehara, Y., Arcila, M., Wang, L., Hasanovic, A., Ang, D., Ito, T., Kimura, Y., Drilon, A., Guha, U., Rusch, V. et al.** (2012). Identification of KIF5B-RET and GOPC-ROS1 fusions in lung adenocarcinomas through a comprehensive mRNA-based screen for tyrosine kinase fusions. *Clin Cancer Res* **18**, 6599-608.

**Takahashi, M., Ritz, J. and Cooper, G. M.** (1985). Activation of a novel human transforming gene, *ret*, by DNA rearrangement. *Cell* **42**, 581-8.

**Takeuchi, K., Soda, M., Togashi, Y., Suzuki, R., Sakata, S., Hatano, S., Asaka, R., Hamanaka, W., Ninomiya, H., Uehara, H. et al.** (2012). RET, ROS1 and ALK fusions in lung cancer. *Nat Med* **18**, 378-81.

**Wirth, L., Drilon, A., Solomon, B., Robinson, B., Lorch, J., McCoach, C., Patel, J., Leboulleux, S., Worden, F., Owonikoko, T. et al.** (2019). Registrational results of LOXO-292 in patients with RET-altered thyroid cancers. *Annals of Oncology* **30**, 933-933.

**Yoh, K., Seto, T., Satouchi, M., Nishio, M., Yamamoto, N., Murakami, H., Nogami, N., Matsumoto, S., Kohno, T., Tsuta, K. et al.** (2017). Vandetanib in patients with previously treated RET-rearranged advanced non-small-cell lung cancer (LURET): an open-label, multicentre phase 2 trial. *Lancet Respir Med* **5**, 42-50.

**Zehir, A., Benayed, R., Shah, R. H., Syed, A., Middha, S., Kim, H. R., Srinivasan, P., Gao, J., Chakravarty, D., Devlin, S. M. et al.** (2017). Mutational landscape of metastatic cancer revealed from prospective clinical sequencing of 10,000 patients. *Nat Med* **23**, 703-713.

## Figures

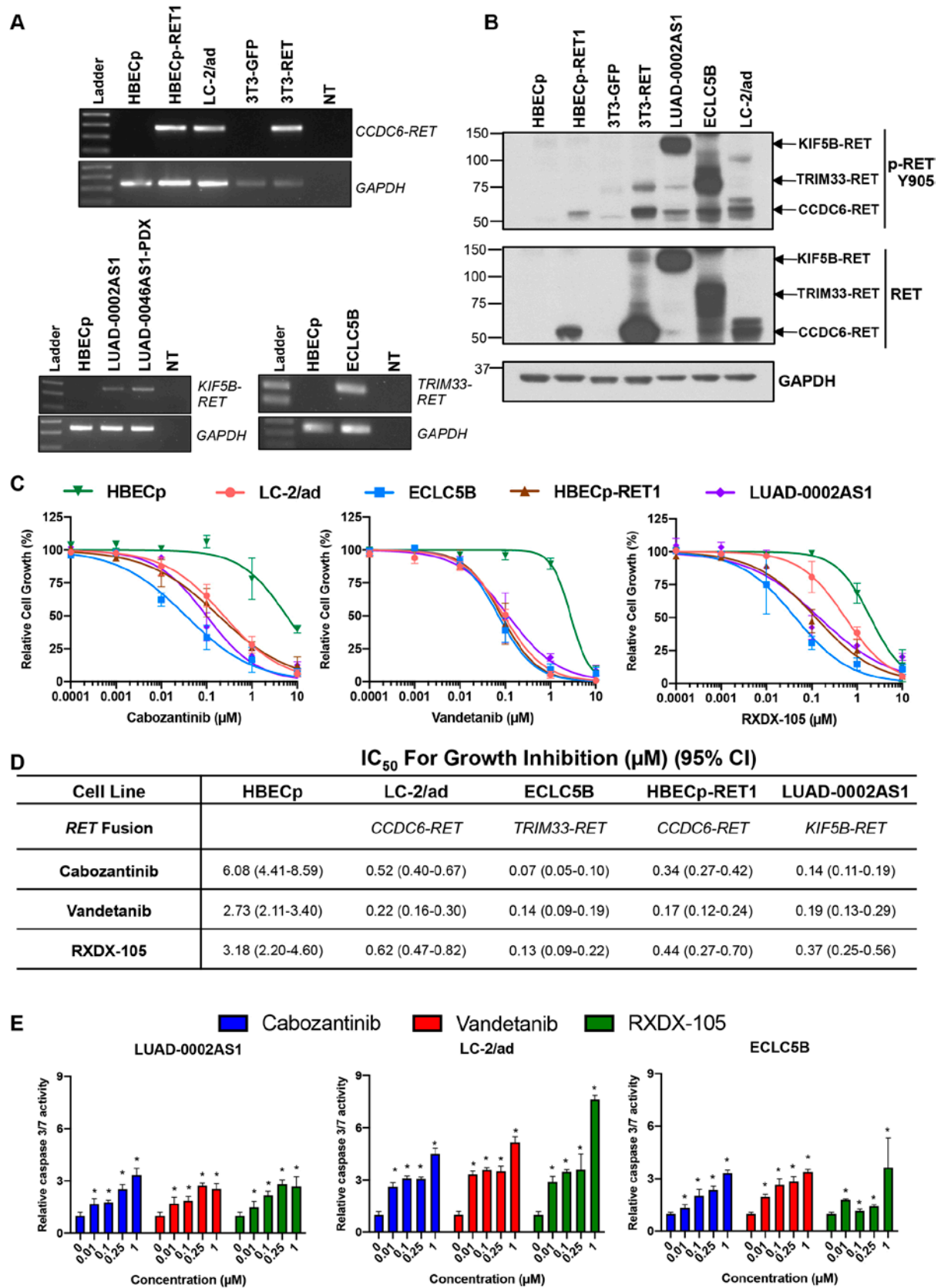


**Figure 1. RET fusion-positive cell lines are sensitive to multi-kinase RET inhibitors.**

**(A).** *RET* expression was confirmed by RT-PCR in LC-2/ad and novel isogenic cell lines. **(B).** Phosphorylation and expression of RET was analyzed by Western blotting in cell lines. **(C).** Cells were starved of serum for 24 h, treated with the indicated concentrations of cabozantinib, vandetanib, and RXDX-105 for 96 h and then cell viability was determined with alamarBlue viability dye. **(D).** Data were analyzed by non-linear regression using Graphpad Prism and  $IC_{50}$  values are shown with the 95% CI in brackets. Data represent the mean  $\pm$  SE of three (RXDX-105 and vandetanib) or five (cabozantinib) independent experiments in which each condition was assayed in triplicate determinations. **(E).** Caspase 3/7 activity. Cells were treated with the indicated concentrations of cabozantinib, vandetanib and RXDX-105 for 48 h and then caspase 3/7 enzymatic activity determined. Results represent the mean  $\pm$  SD of two independent experiments in which each condition was assayed in triplicate determinations. \* $P < 0.05$ , two-tailed t-test. **NT:** no template.

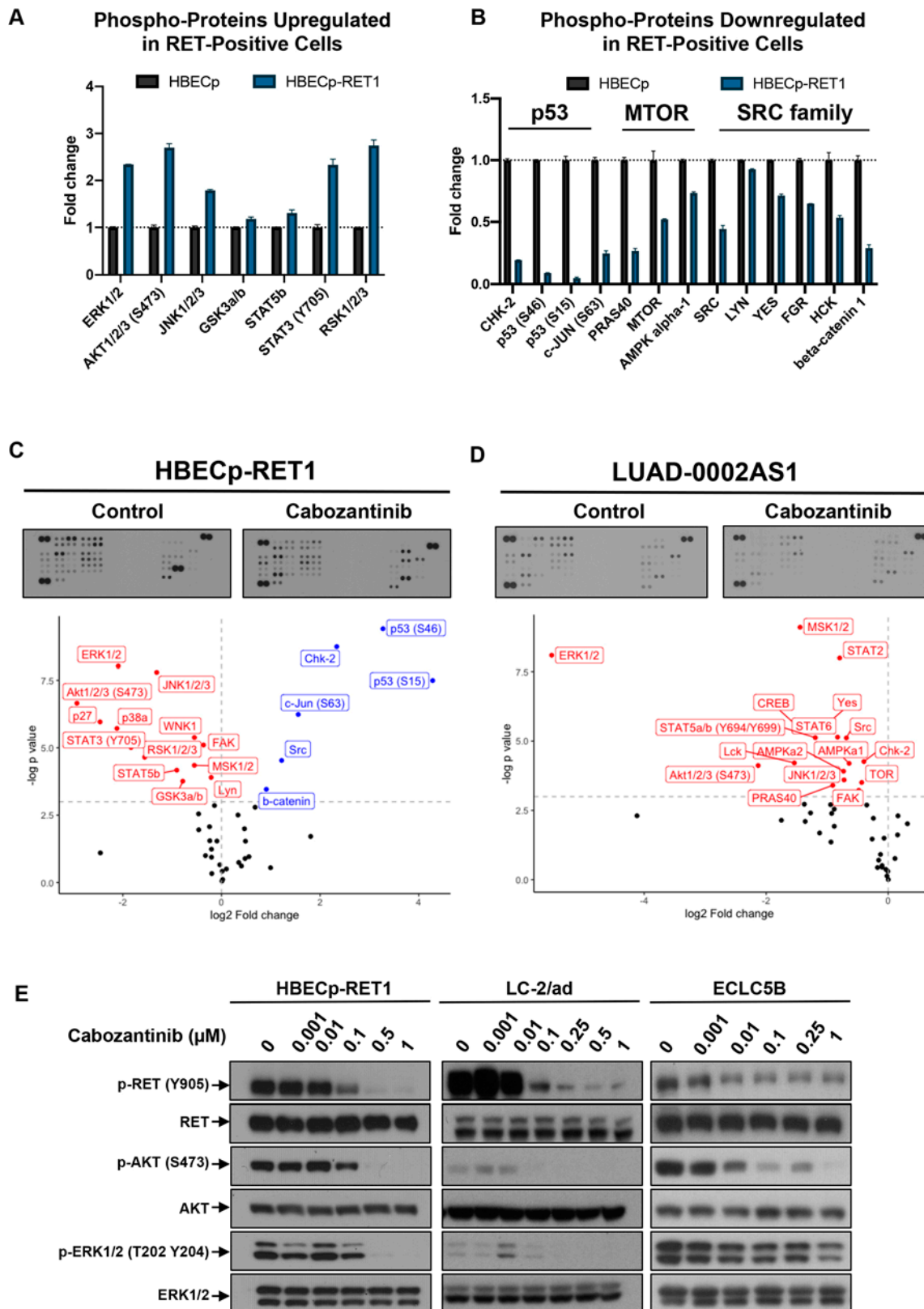


**Figure 2. RET fusions regulate distinct pathways.** Phospho-proteomic profiling was conducted on untreated HBECp and HBECp-RET1 cells in duplicates. The relative change in phosphorylation between the two cell lines is shown as either protein phosphorylation upregulated with CCDC6-RET expression (A) or downregulated following CCDC6-RET expression (B), as quantified from two technical replicates. HBECp-RET1 (C) or LUAD-0002AS1 (D) cells were treated with 0.25 μM cabozantinib for 1.5 h and then phospho-

proteomic profiling conducted on the cell extracts. Phosphorylation was quantitated from two technical replicates and is expressed relative to control (DMSO-treated) cells in the accompanying graphs. Two-tailed t-test was used to calculate the p-value (**E**). Cells were treated with the indicated concentrations of cabozantinib for 1.5 h and then Western blot analysis conducted on cell extracts. Three independent experiments were conducted. Representative immunoblots are shown.

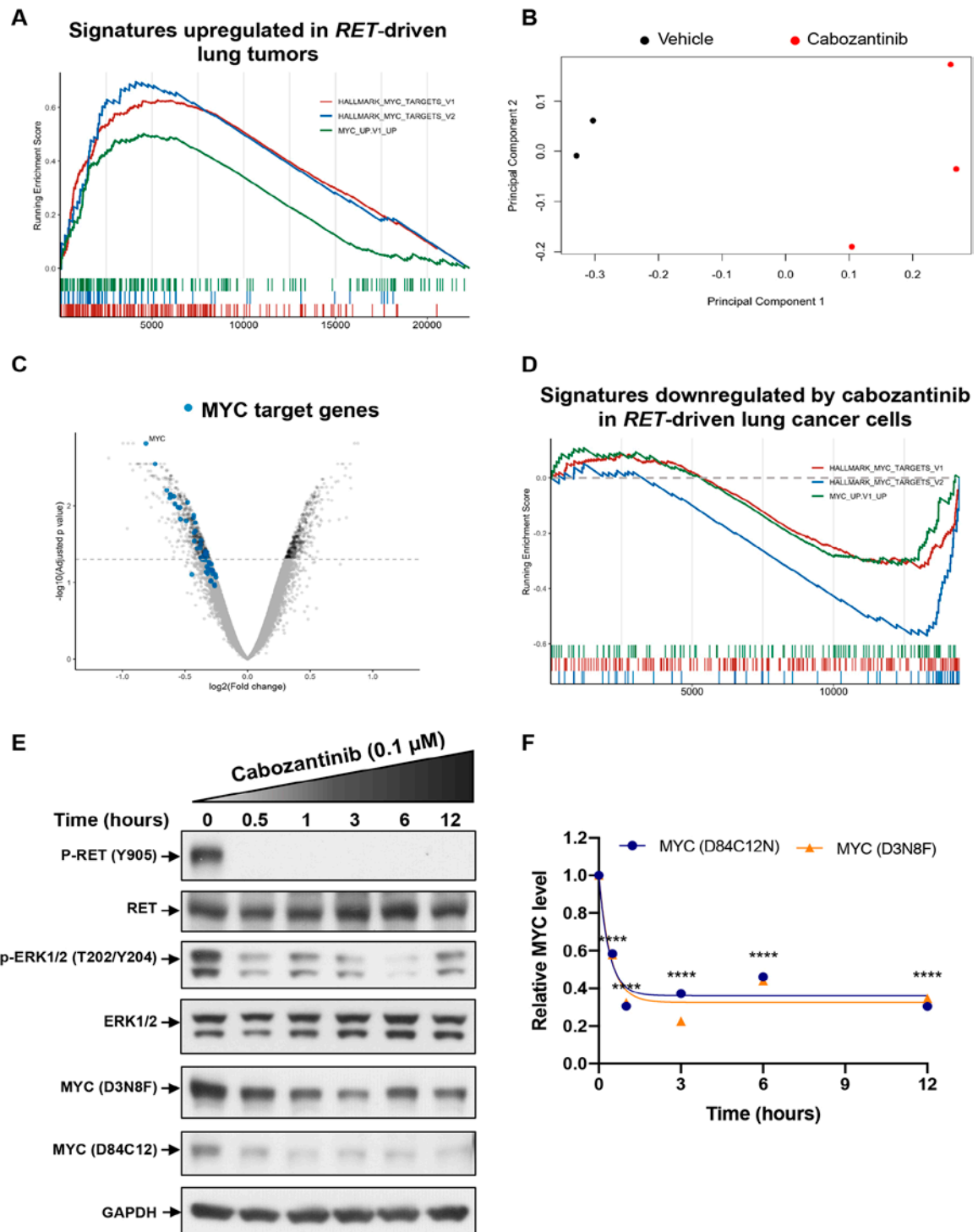


**Figure 3. MYC signaling and expression is regulated by RET in lung cancers with *RET* alterations.** (A). GSEA analysis of the transcriptome of TCGA lung cancer tumors compared with matched normal samples. ECLC5B cells were treated with 0.1  $\mu\text{M}$  cabozantinib for 3 h and the RNA isolated for transcriptomic profiling. Principle component analysis (B), mRNA expression (C) and GSEA analysis (D) are shown. MYC target genes (leading edge genes from HALLMARK MYC TARGETS V1 and V2 combined) are indicated by blue dots. (E and F). Western blot analysis of MYC expression in ECLC5B cells following treatment with 0.1  $\mu\text{M}$  cabozantinib for the indicated times. Representative immunoblots are shown (E). Immunoblots generated using two independent anti-MYC antibodies were scanned ( $n=2$ ) and quantitated, and the half-life for MYC was estimated using GraphPad Prism (F). \*\*\*\* $P < 0.0001$ , two-tailed t-test.

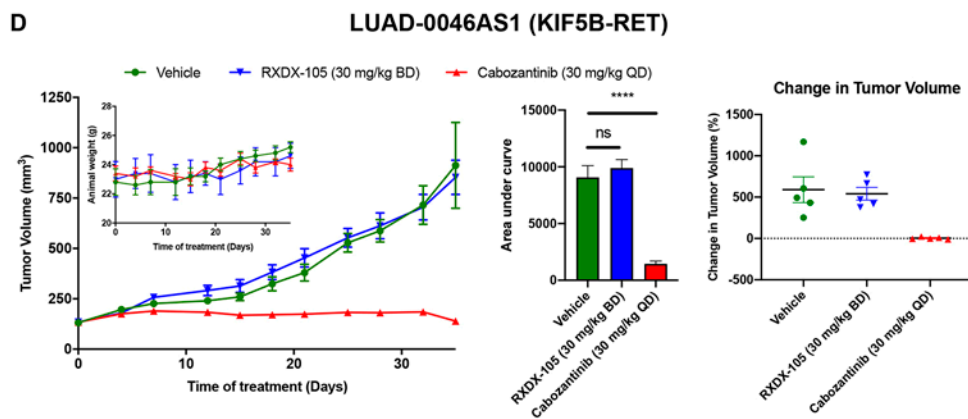
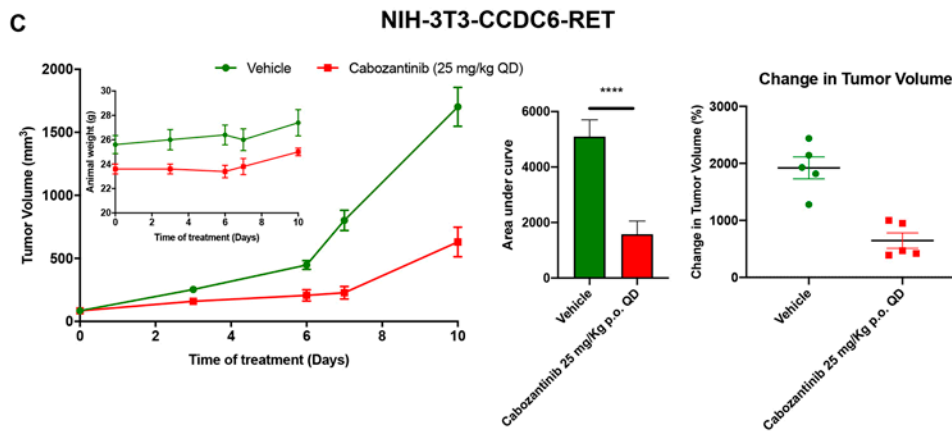
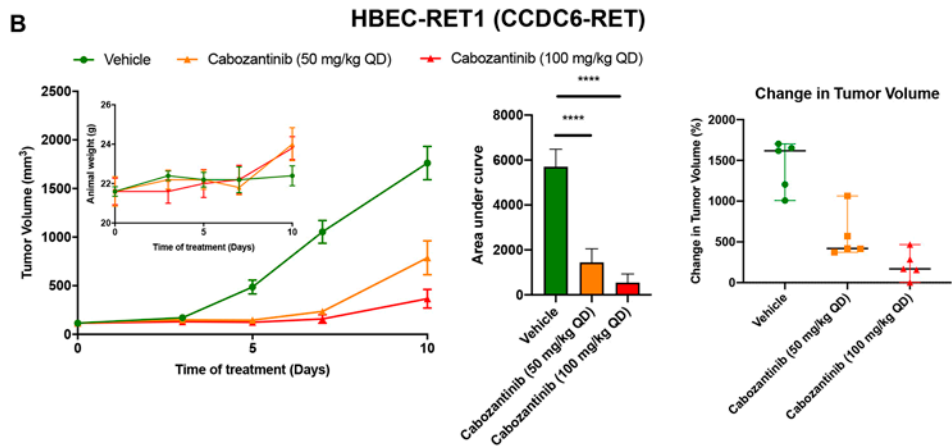
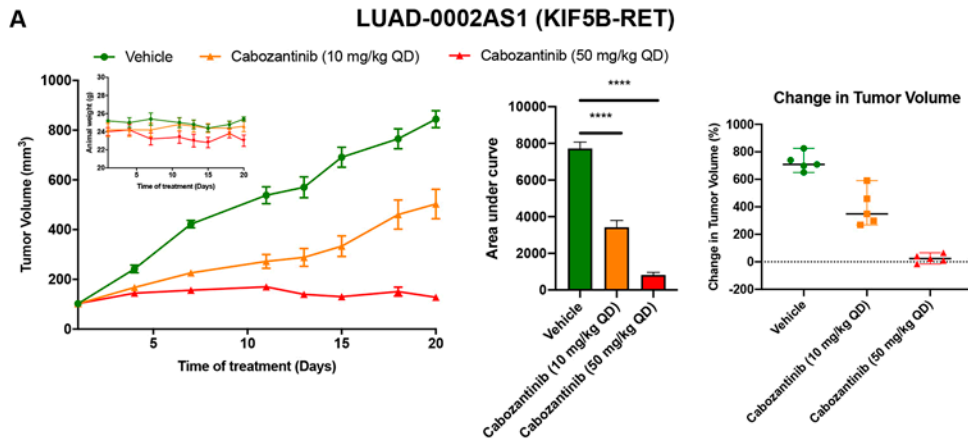


**Figure 4. Cabozantinib inhibits the growth of cell line and patient-derived xenografts and overcomes RXDX-105 resistance in a PDX model.** PDX tumors (**A and D**) or cells (**B and C**) were implanted into the subcutaneous flank of NSG mice and treatment initiated once tumors reached approximately 100 mm<sup>3</sup>. Average tumor volume (left panel), animal weight (left panel, inset), area under curve analysis (middle panel) and the percent change in tumor volume of individual tumors (right panel) are shown. There were 5 mice in each group. Graphs and data analysis were conducted using Graphpad Prism. ns – not significant, \*\*\*\*P < 0.0001, two-tailed t-test.

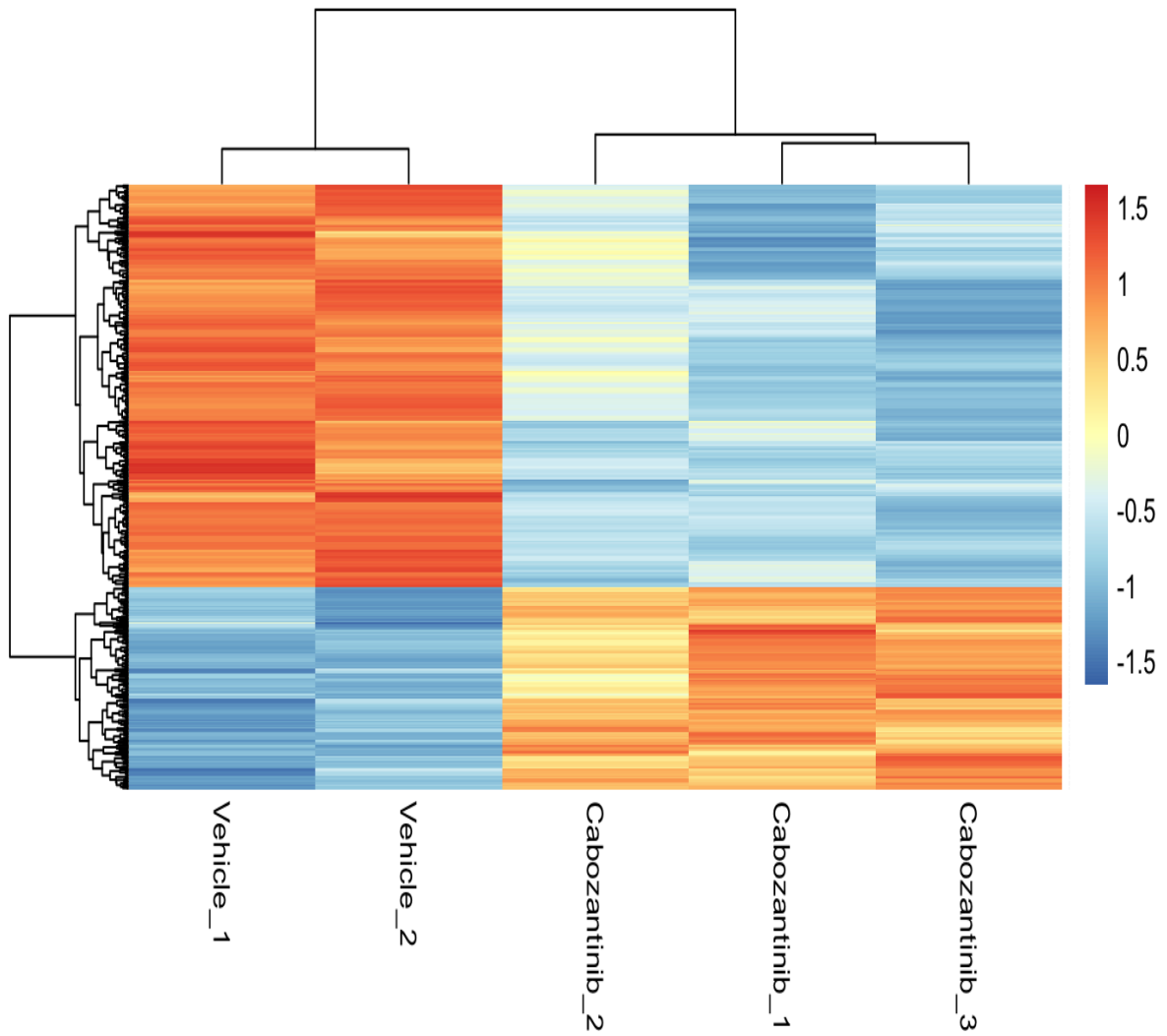


**Figure S1.** Heat map of differential gene expression analysis in ECLC5B cells treated with cabozantinib. Cells were treated with 0.1  $\mu$ M cabozantinib or DMSO for 3 h in triplicates and then RNA extracted for expression profiling.

Table S1

[Click here to Download Table S1](#)

Table S2

[Click here to Download Table S2](#)

Table S3

[Click here to Download Table S3](#)

Table S4

[Click here to Download Table S4](#)

Table S5

[Click here to Download Table S5](#)

Table S6

[Click here to Download Table S6](#)